13th International Conference on
Structural Health Monitoring of Intelligent Infrastructure
DOI: 10.3217/978-3-99161-057-1-007

Monitoring of fatigue crack propagation by means of distributed fiber optic sensing

Petr Dohnalík[1], Stefan Lachinger[1], Maciej Kwapisz[1], Alois Vorwagner[1]
[1] Transportation Infrastructure Technologies, Austrian Institute of Technology,
Giefinggasse 4, 1210 Vienna, Austria
email: Petr.Dohnalik@ait.ac.at, Stefan.Lachinger@ait.ac.at, Maciej.Kwapisz@ait.ac.at, Alois.Vorwagner@ait.ac.at

ABSTRACT: Distributed Fiber Optic Sensing (DFOS) is an innovative technique for Structural Health Monitoring (SHM). Taking advantage of the fact that DFOS can conveniently measure mechanical strain continuously along an optical fiber, it is increasingly used in monitoring of concrete bridges and tunnels. However, DFOS still needs research in new application areas, such as monitoring of steel bridges. In the present study, DFOS is used to investigate the potential to monitor fatigue crack initiation and propagation by experiments. In a full-scale test, a steel railway bridge was dynamically excited into resonance, generating fatigue-effective vibration amplitudes. The fiber was glued to the flange of the main beam in several loops to cover a larger area for crack detection. The measured strain signal was compared with results obtained from Finite Element Method (FEM) simulations supported by data acquired from conventional strain gauges and extensometers. The strain measurement with DFOS showed excellent agreement with the simulated strain. In this context, additional information about crack initiation, propagation, opening and length can be obtained indirectly from the DFOS measurement. However, when the crack is crossing the fiber, nonlinear effects come into play. To consider the nonlinear effects, a hysteresis model taking steel-fiber interaction into account was applied. The results of the study are presented and the applicability and potential of DFOS for fatigue crack monitoring in railway bridges is discussed.

KEYWORDS: Distributed Fiber Optic Sensing; Structural Health Monitoring; Crack propagation; Steel railway bridge; Finite Element Method; Dynamic excitation.

1 INTRODUCTION

Structural health monitoring of fatigue cracks in steel bridges aims to detect and evaluate cracks as early as possible before they can cause serious consequences. The current well-established method for detecting and monitoring fatigue cracks is visual inspection, which does not necessarily imply crack detection due to its inherent limitations [1]. Conventional extensometers, vibrating wire sensors, or strain gauges are well suited for monitoring only a small area of a component. This is suitable for monitoring of known cracks, but not for detecting new cracks [2].

To overcome the drawbacks of these methods, various sensors and monitoring techniques have been proposed. For example, a soft elastomeric capacitor that monitors a particular area of interest [3], coating sensors that use the change in potential difference [4], or the strain-based method employs fiber optic sensors [5].

When it comes to crack monitoring along bridges, the ability to simultaneously measure strain along a fiber, is the main advantage of the DFOS technique over other sensors that utilize different measurement principles [2].

The measurement principle of distributed fiber optic sensing is based on the backscattering of light sent through an optical fiber. Changes in temperature and mechanical strain lead to changes in the characteristics of the backscattered light, which are evaluated by reflectometer [1], [2], [6]. Rayleigh, Raman, and Brillouin scattering are commonly studied and mentioned in the scientific literature as types of scattering, where Rayleigh type achieves much higher spatial resolution and it is preferred for crack monitoring and micro-damage detection [1].

Spatial resolution is one of the most important factors in DFOS measurement. It can be thought of as the fiber being divided into small virtual gauges. The distance between the two closest gauges is also known as the “gauge pitch” (the term “gage pitch” is used interchangeably in the literature). In this study, the finest available spatial resolution of 0.65 mm can be used with up to 20 m long fibers [7]. The spatial resolution decreases with increasing fiber length or sampling frequency. Small gage pitches should be preferred in regions with large strain gradients, such as around cracks [1]. However, if the strains or strain gradients are too high and exceed the technical capabilities of the interrogator, the measurement software will replace unreliable values with not a number (NaN) value, also known as dropouts. Dropouts can also occur in the area of small bending radius, poor terminations, at the fiber splices, or due to high frequency effects during vibration [1].

The DFOS technique has found application in broad range of industries. One example can be taken from the structural health monitoring of a prestressed concrete highway bridge in Austria [8]. The authors took advantage of this DFOS technique to monitor mechanical strains and temperatures of approximately 2×30 m long bridge sections during the construction process. Within the observed time period, several cracks resulting from concrete shrinkage were detected. DFOS also allowed to observe the cracks closing while prestressing.

To the best knowledge of the authors, it is identified that the investigation of the crack propagation in a steel bridge under cyclic loading by means of DFOS remains unexplored. The present contribution wants to explore this possible new application and wishes to close this knowledge gap.

DOI: 10.3217/978-3-99161-057-1-007

2 MATERIALS AND METHOS

The bridge investigated in this study was a steel railroad bridge built in 1953 and decommissioned in 2022. The single-span girder bridge with a length of 21.5 m and a width of about 2.2 m (after cutting the sidewalks) was transported as a whole, with crossties and rails, to the test site of the Austrian Federal Railways (ÖBB) in St. Pölten, see Figure 1, where it was subjected to an experimental campaign.

Figure 1: Pinkabach Bridge without sidewalks at the ÖBB test site.

2.1 Loading and investigated areas of the Pinkabach Bridge

Six concrete blocks, each weighing 11 tons, were placed on top of the rails to ensure that the minimum and maximum peaks of the imposed harmonic loading were always in tension. Harmonic excitation near to the bridge's natural frequency was applied using a large hydraulic exciter, the Mobile Seismic Simulator (MoSeS), provided by Austrian Institute of Technology (AIT). The amplitude of the imposed harmonic loading was intended to be on the same level as the maximum amplitude of a passing train.

Two critical areas (details) of the bridge were considered in this investigation. These were located on the lower right and left flanges near the transverse plane of symmetry of the bridge, see Figure 2. The right and left locations of interest are further referred to as Q3R and Q3L, respectively.

In order to initiate a fatigue crack at these locations, a notch was made on each side by an angle cutter near the gusset plates of the girders, which were used to attach the transverse and diagonal struts inside the bridge. At the Q3R location, the notch was 150 mm away from the symmetry plane; at the Q3L location, the notch was 360 mm from the transverse symmetry plane. Both notches were about 30 mm long and 3 mm wide.

2.2 Conventional measurement techniques

The experimental methods relevant to this study consisted of conventional strain gauge and extensometer measurements, positioned as shown in Figure 3. The latter allowed the measurement of crack openings, while the strain gauges provided information on the strain response of the structure due to the harmonic excitation. The strain oscillations were recalculated to stresses and the cyclic stress levels were evaluated using the rainflow counting algorithm. These results served as: i) an input for fracture mechanics calculations and ii) comparative values for the innovative DFOS application.

The strain gauges for ferritic steel 1-LY41-6/120 (HBK GmbH, Germany) were attached to the underside of the flanges directly below their webs, 800 mm from the transverse plane of symmetry, see DMS positions in Figure 2. Two extensometers K-WA-U020W (HBK GmbH, Germany) were installed at the tips of the notches on the left and right sides of the bridge. It should be noted that the mounting points of the extensometers were 40 mm away from the notch tip (80 mm from each mounting point), as indicated by the two crosses in Figure 3.

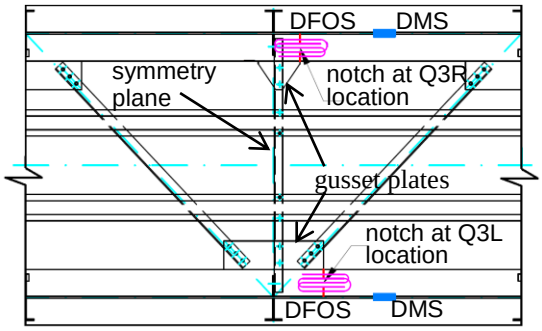

Figure 2: Top view of the central area of the Pinkabach Bridge plan showing the arrangement of the strain gauges, DMS (marked by blue rectangles), and DFOS fibers (pink loops) near the gusset plates.

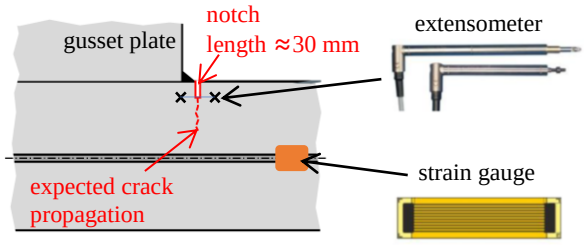

Figure 3: Detailed scheme of the conventional measurement instruments installed near the center of the girder. Source: TU Graz, Hottinger Brüel & Kjaer GmbH.

2.3 DFOS measurement technique

Two polyimide optic fibers (Polytec GmbH, Germany) were glued (Loctite EA 3430, Henkel AG, Germany) at the Q3R and Q3L locations in front of the cut notches where crack initiation and propagation were expected. The fibers were laid in multiple loops on the underlying flange and are referred to as fiber sections 1 to 5, numbered ascending from the flange edge. Due to the minimum allowable bend radius of the fiber, the order of the acquired signal by ODiSI 6000 interrogator (Luna Innovations Inc., USA), differs from the section numbering and corresponds to the winding of the loops that as illustrated in Figure 4. An example of the received signal from the five sections and their numbering is shown in Figure 5.

2.4 Linear FEM modeling of the DFOS measurements

The arrangement of the notched flange with a crack and an optical fiber was represented as a finite element method (FEM) model. The Ansys Mechanical Solver (Ansys Inc., USA) was used together with APDL coding to perform linear elastic calculations. In order to facilitate the manipulation and parameterization of the model and to speed up the calculations, a 2D FEM model was used to carry out the main numerical

DOI: 10.3217/978-3-99161-057-1-007

simulations. Since the Q3R and Q3L locations are at very similar positions with respect to the length of the bridge, the 2D FEM model with the same geometry was used for both Q3R and Q3L locations.

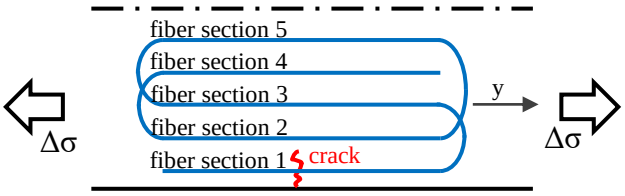

Figure 4: Schematic representation of the half-flange with the fiber winding layout in relation to the fiber section numbering. The dash-dotted and the continuous lines represent the web and the edge of the flange, respectively. The arrows indicate the uniaxial tensile stress state.

One of the most important parameters investigated in this study is the crack width, also referred to as the crack opening. Because the crack opens in the longitudinal direction of the flange (*y*-direction as shown in Figure 4), the contribution of the web to the girder stiffness was investigated as it is expected to have the most influence affecting the results of the 2D FEM model. In this context, the crack openings of the 2D model were compared with the 3D FEM model of the main longitudinal girder of the Pinkabach Bridge. The motivation was to investigate the effect of the absence of the web and the upper (compressed) flange on the stiffness of the 2D FEM model. This is described in more detail in Section 2.7.

2.5 Linear 2D FEM model of cracked flange and DFOS optical fibers

The geometry of the flange was modeled as a rectangle 400 mm wide, corresponding to the width of the flange, and 600 mm long, which is long enough to have a uniform stress state at its ends. The shape of the notch does not affect the calculated crack widths. Therefore, it was not accounted for in the present study and only the material discontinuity was considered, i.e., the nodes on the axis of symmetry located at the position of the crack were allowed to move freely. The fibers were modeled as beams with a thickness of 0.5642 mm at each position, taken from [2].

The flange mesh was generated with 8-node quadrilateral PLANE183 elements using plane stresses with a thickness option [9] corresponding to the flange thickness. A mapped mesh with an element size of 5 mm and 1 mm in the longitudinal and transverse directions, respectively, was applied to the flange. The optical fibers were meshed using a three-node BEAM189 element with quadratic shape functions [9]. The length of the beam elements was 5 mm, and the position of the nodes coincided with the nodes of the flange. COMBIN14 elements [9] were used as spring elements connecting the coincident nodes of the flange and optical fibers and representing the glue between these two components. The COMBIN14 elements were used for nodes that were more than 5 mm away from the axis of symmetry.

The boundary conditions for the optical fibers were as follows: the nodes of the fibers lying on the axis of symmetry were constrained in their longitudinal displacement as well as in their total rotation. On the other side of the flange, the last nodes of the beam elements were coupled in all directions to their corresponding elements of the flange. The nodes of the flange that were on the axis of symmetry were constrained in the longitudinal direction, where there was also a fixed material on the other side. There was no constraint for the nodes in the cracked area, i.e. the crack length is controlled by the constraining the displacements of the nodes in the *y*-direction. One node on the symmetry axis, located in the center of the flange, was also constrained in transverse direction.
The tensile load was applied in the form of pressure on the shorter edge opposite to the axis of symmetry. The geometry, mesh and boundary conditions are shown in Figure 6.

The material properties of the components were linear elastic. For the steel flange, standard elastic properties were used with a modulus of elasticity of 210 GPa and a Poisson's ratio of 0.3. The glass fiber was assigned a modulus of elasticity of 30 MPa and a Poisson's ratio of 0.3 [2]. The elastic modulus of the glue was initially unknown and it was subject of the investigation. After the investigation, a modulus of elasticity of 900 kPa was assumed.

2.6 Linear 3D FEM model of the main girder

The 3D FEM model simulates a crack in the flange of one of the main girders of the Pinkabach Bridge. The girder length, web height, web thickness, flange thickness, flange width of the girder amount to 21500 mm, 1875 mm, 14 mm, 30 mm, 400 mm, respectively.

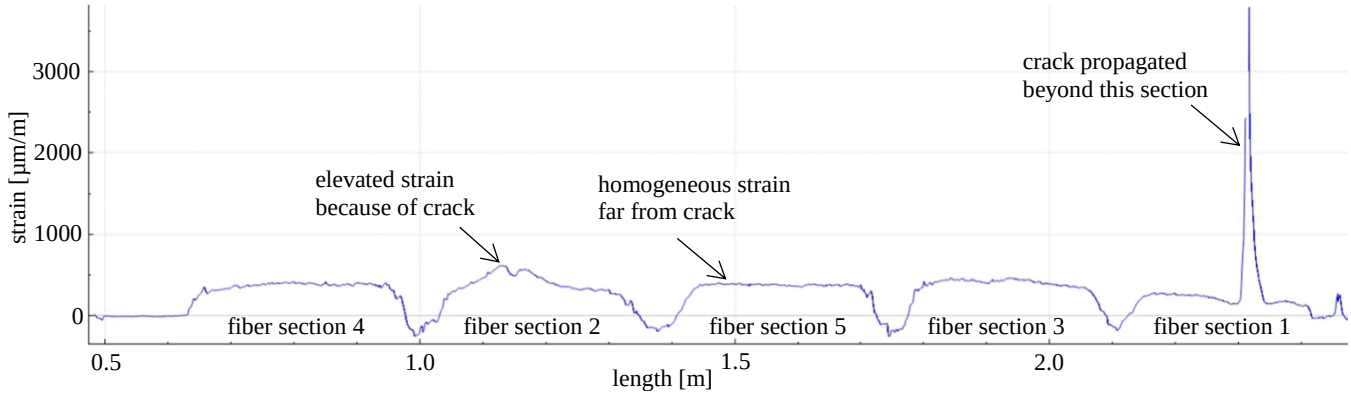

Figure 5: An example of the acquired strain signal along the fiber at a specific time instance. The plateaus of the received signal correspond to the straight fiber sections shown in Figure 4.

DOI: 10.3217/978-3-99161-057-1-007

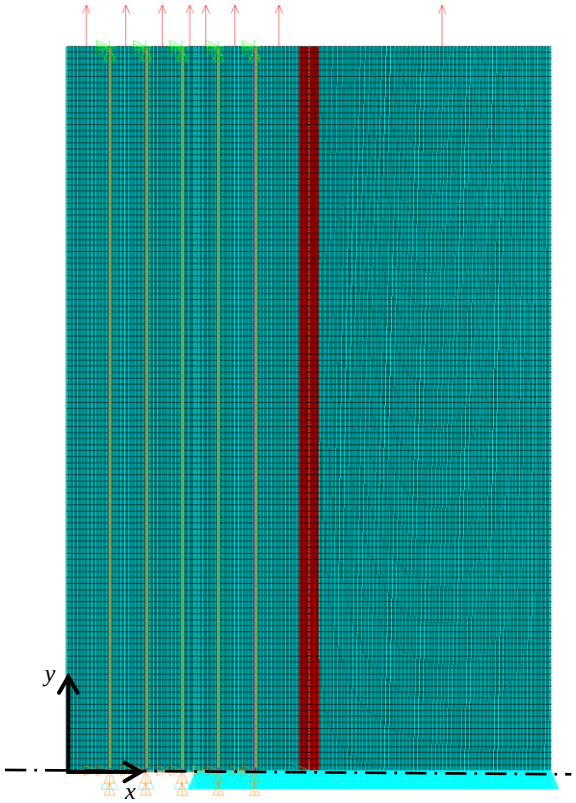

Figure 6: The 2D FEM model of the cracked flange. The dashed line corresponds to the transverse axe of symmetry; the blue rectangles represent finite elements; the red rectangles mark the area of higher web stiffness; the yellow vertical lines mark the optical fibers. The blue rectangles on the symmetry axis indicate the boundary condition for the displacement. The orange rectangles applied to each fiber ending on the axis of symmetry are rotational constraints, while the green triangles correspond to coupled nodes between the fiber and the flange. Red arrows indicate the direction of the applied stress.

The flanges as well as the web were meshed by SHELL281 elements with quadratic base functions [9]. Around the notch, the mesh was finer than in the rest of the girder and its properties are the same in terms of element type and element size. Outside of the fine area, a coarse mesh was used. As for the web, elements with a length of 697 mm and a width of 127 mm were used. For the coarse part of the flange, the elements were 697 mm long and 200 mm wide. Mapped mesh with quadrilaterals was used on most of the girder geometry, as shown in Figure 7.

The boundary condition of the 3D FEM model was analogous to a simple supported girder, corresponding to suppression of longitudinal, and vertical displacements of the nodes at the short edge of the lower flange (with crack) on one side and the suppression of vertical displacements along the edge of the other side, see Figure 7. In addition, one node in the middle of the edge of the bottom flange at the end is constrained in transverse direction.

The loading of the numerical 3D FEM model was carried out by a single point force in the middle of the upper flange. The elastic material properties of all parts used in the 3D FEM model were the same as in the 2D model.

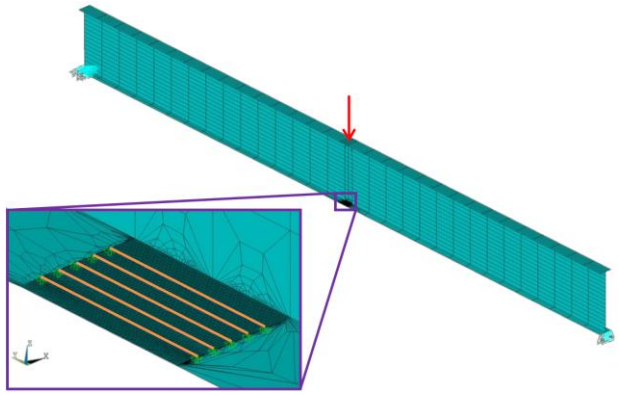

Figure 7: The 3D FEM model of the Pinkabach Bridge main girder with cracked flange and DFOS fibers. The displacement boundary condition, and the point load are marked by blue triangles and red arrow, respectively. The detail of the fine-mesh area with crack and DFOS fibers (yellow lines) is shown in the lower left.

2.7 Comparison of the linear 2D and 3D FEM models: web stiffening factor

The crack openings of the 2D FEM model were compared with those of the 3D model in order to investigate the influence of the absence of the web in the 2D model. This absence was manifested by a higher crack opening of the 2D model, indicating a lower stiffness of the 2D model. As a remedy, a strip of higher stiffness than the surrounding steel was inserted to the 2D FEM model. This strip is 14 mm wide and is located in the middle of the flange, geometrically corresponding to the footprint of the web, see the red area in Figure 6. The modulus of elasticity of the strip was expressed as a multiplication factor to the surrounding steel with a modulus of elasticity of 210 GPa. Depending on the crack length, higher elastic moduli were assigned to the strip in order to match the crack openings of the 3D and 2D models. The multiple of the higher steel elastic modulus of the strip is referred to as the web stiffening factor in this document.

The procedure for finding the web stiffening factor was as follows:

i) Find the single point load of the 3D model (red arrow in Figure 7) that yields the same stress of 50 MPa in the homogeneous stress field in the vicinity of the notch (with crack length = 0) of the 2D and 3D models.
ii) After harmonizing the homogeneous stress fields in the vicinity of the notch and finding the point load of the 3D model, the distance between the two corner nodes at the very end of the notch was measured. This ”notch opening” was compared to the 3D and 2D models.
iii) The strip stiffness of the 2D model (red area in Figure 6), which caused the same “notch opening” in the 2D and 3D models, was expressed as a multiple of the steel stiffness of 210 GPa. In this way, the web stiffening factor was obtained.
iv) The crack length behind the notch tip was increased by a certain increment, and the step iii) was repeated.

The web stiffening factors were obtained for crack lengths from 0 mm up to 160 mm by means of repeating steps iii) and iv). The increments for crack lengths from 0 mm to 140 mm were 20 mm, and for crack lengths from 140 mm to 160 mm

DOI: 10.3217/978-3-99161-057-1-007

were 10 mm. The web stiffening factors as a function of crack length are plotted in Figure 8.

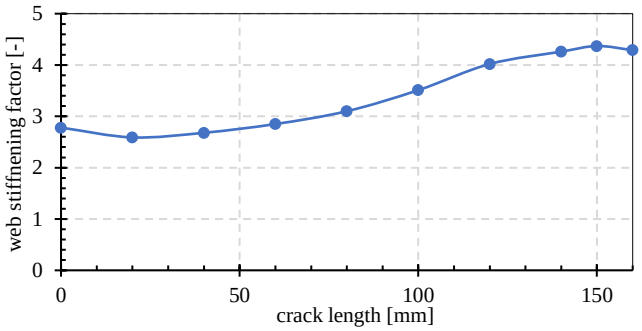

Figure 8: Web stiffening factors as a function of the crack length. Web stiffening factors are the multiples of the flange steel elastic modulus assigned to the strip in the 2D model.

2.8 Modeling the glue between the flange and optic fibers

The glue bonds the DFOS optical fiber with the underlying steel flange, see Figure 9 a). In the linear FEM models, this bond was modeled by linear springs characterized by their stiffness, see Figure 9 b). The springs connect coincident nodes of the flange and the fiber. The springs were active in the *y*-direction, the longitudinal axis of the flange. In the FEM models, the first spring was located 5 mm away from the symmetry axis. The next springs connected the flange and fibers from this point to the end of the fiber where the flange and fiber nodes were coupled, see Figure 6.

The stiffness of the glue was investigated based on experience from previous work [2] and the current DFOS measurement. Softer springs (i.e., softer glue) produced flatter strain peaks when the crack was close to the fiber. Increasing the stiffness caused the calculated strain response curve to become narrower, see Figure 9 c). The calculated strain response from the 2D model was compared to the measured DFOS signal. A glue stiffness of 900 kPa gave satisfactory agreement between the calculated and measured strain shapes and was used in further calculations.

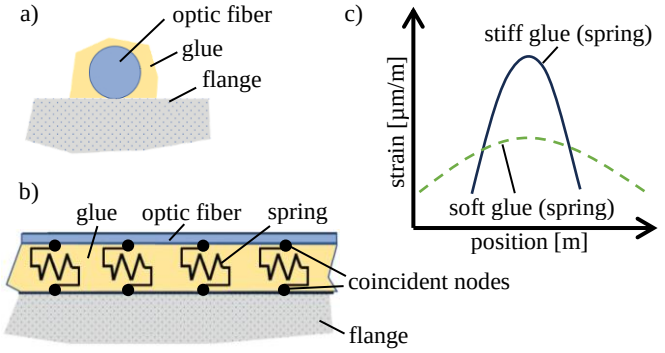

Figure 9: Detailed sketch of a) cross-section of the bond between fiber, glue, and the flange, b) glue being represented as linear springs connected to coincident nodes (zero glue thickness). c) strain response corresponding to soft glue (dashed curve) and hard glue (orange curve).

2.9 Nonlinear hysteresis model for determining crack width

The linear FEM model, simulating the strain distribution from the glass fiber to the underlying object, is able to reproduce the measured values up to the crack formation. However, as it will be shown in the result section, once the crack reaches the fiber, there is no longer sufficient agreement and the strain from the linear FEM model deviates more and more from the measured values as the crack increases in size. This is due to nonlinearities in the fiber and the glue that occur at very high strains and can no longer be represented by the linear model.

Although this phenomenon is known from earlier studies, as explained in [2], the physical background has not yet been clarified in detail. The most likely explanation is a permanent mutual displacement between fiber and base material in the glue layer (sliding), which occurs after exceeding the mutual friction, or plastic deformation of the optical fiber. A mechanical model based on this hypothesis had already been developed by the AIT research group and proved to be very effective. It allowed the strain behavior to be simulated with a high degree of accuracy under various loading and unloading scenarios and crack widths of up to 2.8 mm.

An overall model of the optical fiber structure and the glue was adopted from [2], with the parameters being slightly adjusted to the actual fiber used. This model makes it possible to calculate the interaction of these elements and also to calculate non-measurable strain signal during high-frequency excitation with large crack widths (high amplitudes) using FE methods. The hysteresis model consists of a combination of linear and nonlinear spring and beam elements. The fiber structure, including the connecting elements, is shown in Figure 10 a) and b). The glue (3) is modeled as a linear spring, while the coating (2) and the fiber (1) are defined as 1D beam elements. The crucial connection between the fiber and the coating is modeled by nonlinear springs (4). This is an elasto-plastic spring element whose force F increases linearly with the deformation V and the stiffness k_{int} up to the limit force F_S. After the limit force F_S is exceeded, slippage V_{SL} occurs as a permanent displacement of the fiber optic cable (1) relative to the coating (2), see Figure 10 c).

The model was implemented in the FE program Ansys, whereby, in contrast to the linear model, only a 20 cm long section around the crack and only one fiber at a time is considered separately. The aim of this investigation is to interpret the measurement signal and to draw conclusions about the crack width. During the interpretation, it can be determined whether the crack is currently closing or opening or whether a larger crack has occurred previously. It is not necessary to apply the nonlinear model to recalculate the crack width if a complete, continuous measurement signal is available, as the crack width can be calculated by integrating the signal over the fiber length. Since it is known that transient or permanent dropouts can occur at higher amplitudes and higher excitation frequencies, this step is important to significantly increase the accuracy of the crack width determination.

In the present case of the linear model described in Section 2.8, a fiber without a coating was used, which theoretically results in differences to the model shown in Figure 10, as the comparison with the simplified model in Figure 9 shows. However, since comparable nonlinear effects occurred in the measurement data despite the absence of the fiber coating, the model described in [2] was also applied here and showed good results.

DOI: 10.3217/978-3-99161-057-1-007

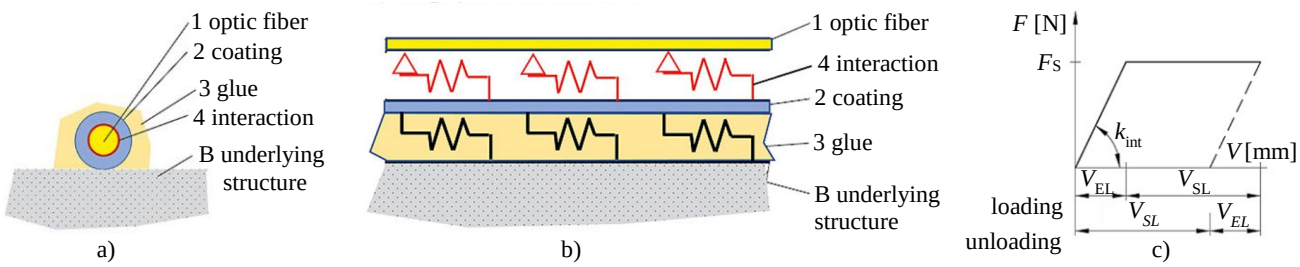

Figure 10: Schematic drawing of a) cross section and b) side view of the nonlinear model used to estimate the crack width; c) the material model prescribed to the springs where slippage is initiated when the force F exceeds the limit force F_S.

This is also due to the fact that the model parameters were not determined individually, but were found empirically from the measurement data by model fitting as an overall model. These determined characteristic values in Table 1 thus do not represent any physical material parameters, but the overall structure including the glue. These characteristic values determined in this way are not transferable to other fiber applications, even with the same fiber, without slight adjustment.

Table 1: Input parameters for the nonlinear FE analysis.

element size	glue (spring)	coating (beam)	interaction (spring)	glass fiber (beam)
2 mm	K = 10^6 N/m^2	A=10^{-4} m^2 E=30 MPa	K=7·10^6 N/m^2 F_s=0.35 N/m	A=10^{-5} m^2 E=30 MPa

3 RESULTS

3.1 Crack width vs. crack length under unit load

One of the main results of this study is the relationship between crack width and crack length. Since the problem is modeled with linear elasticity, it is reasonable to do this for a unit load. The calculations were carried out using the 2D model.

The crack widths were obtained for the following locations: at the notch tip (x = 30 mm), at the fiber locations, at the location of the crack tip, and the notch tip (x = 30 mm), but 40 mm above the axis of transverse symmetry of the 2D model (y = 40 mm). This location corresponds to the extensometer mounting points. The crack widths were determined for crack lengths from 0 mm to 160 mm with 5 mm increments. For each calculation, the appropriate web stiffening factor was taken into account. The results are shown in Figure 11. It is noteworthy, that the extensometer reading is non-zero even for zero crack length, which is caused by the elasticity of the steel between the extensometer mounting points.

3.2 Comparison of crack growth and fracture mechanics

As part of the test evaluation, a fracture mechanics analysis of the fatigue tests on the Pinkabach Bridge was carried out by the scientific partner, the Institute of Steel Structures of the Technical University Graz (TU Graz), which also included the evolution of the crack length over the number of cycles for the two locations Q3L and Q3R shown in Figure 12. This fracture mechanics analysis is compared to the crack width vs. crack length relationship derived from the 2D FEM model in the previous Section 3.1, shown in Figure 11.

In order to perform this comparison, the number of cycles was determined at each measurement time instance. At this particular measurement time instance, the crack length was determined using Figure 11 and the extensometer reading. This crack length and number of load cycles were entered into the fracture mechanics diagrams in Figure 12.

Comparison with the fracture mechanics analysis "best fit" (green curve) shows reasonable agreement, although it is not perfect. The numerical results tend to be slightly higher than the fracture mechanics results for short crack lengths. For long crack lengths, however, the numerical results are slightly lower than the fracture mechanics results. There are uncertainties in both, the fracture mechanics analysis and the numerical analysis, and it is expected that there will be differences. For example, a complete 3D model of the main girder including the gusset plates, and the influence of the bracing would allow a more accurate analysis. However, the method is considered to be adequate for estimating the crack length for practical construction purposes based on simple extensometer readings.

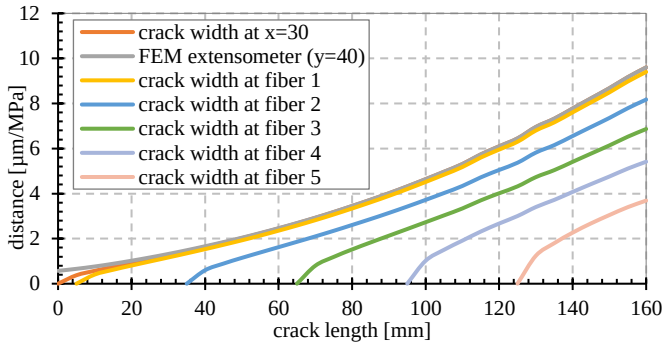

Figure 11: Crack width as a function of crack length; FEM extensometer corresponds to the displacement reading at the location of the extensometer attachment, i.e.: at the notch tip (x = 30 mm from the flange edge) and y = 40 mm above the axis of transverse symmetry of the 2D model.

3.3 Comparison of the linear 2D FEM model with the DFOS measurement at the Q3R and Q3L locations

The strains calculated by the 2D FEM model, to which the conventional experiments provided input, are compared in side-by-side plots with the DFOS strain signal at multiple time instances throughout the experimental campaign. The results from the 2D FEM model at a time instance were obtained in 3 steps. First, the loading stress was determined as the difference between the minimum and maximum amplitude readings from respective strain gauge at the corresponding time instance, multiplied by the modulus of elasticity of 210 GPa. Second, the crack length was extracted from Figure 11 (FEM extensometer), by knowing the displacement reading of the extensometer divided by the loading stress derived from the

DOI: 10.3217/978-3-99161-057-1-007

strain gauge reading for the corresponding time instance. Third, the applied stress and crack length were used as input for the FEM simulations.

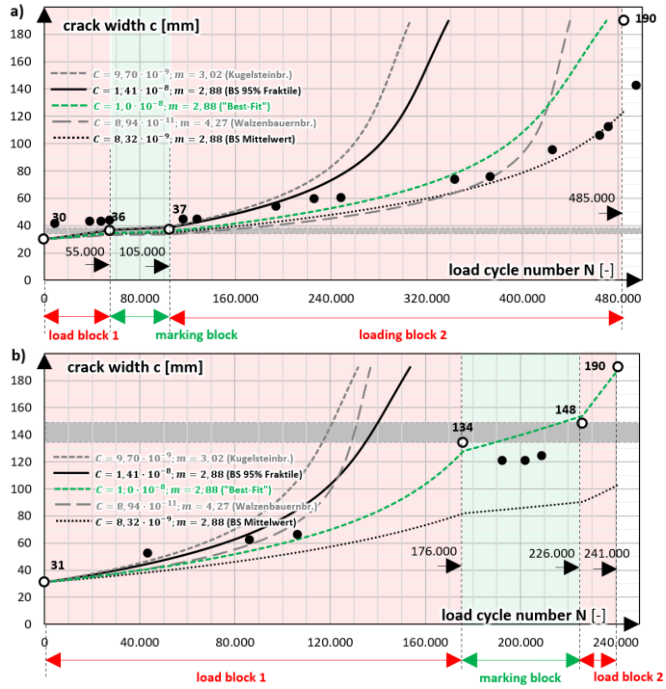

Figure 12: Fatigue calculations provided by TU Graz showing the crack length as a function of the number of load cycles for the two locations: a) Q3R and b) Q3L; the solid black circles show the results derived from the linear elastic FEM model; the monotonically rising curves correspond to different fatigue models. Credit: TU Graz.

The measured DFOS signal used for comparison with the numerical simulations was obtained by subtracting the minimum DFOS signal (red graph in Figure 13) from the consecutive maximum DFOS (green graph in Figure 13) signal for the corresponding time in order to account for the mean strain value (blue graph in Figure 13). In this way, the difference between the numerical and measured signals is "tared", and they can be directly compared. The elevated strain values reminiscent of plateaus in this blue graph correspond to individual fiber sections. The order of the fiber sections is the same as shown in the Figure 4 and Figure 5.

An example of a typical comparison of the measured and simulated strain signals at fiber section 5 is shown in Figure 14, where the signals are almost identical. It was observed that when the fiber is far away from the crack tip, the measured and simulated signals are in good agreement.

The measured DFOS signal indicates that the cracks were already present near the fiber section 1 already on the first day of measurements at both Q3R and Q3L locations. At this time, it can be seen that the simulated and measured signal amplitudes do not match each other, see Figure 15. This suggests that a nonlinear effect is at play, which may be caused by the interaction between the optic fiber, coating, glue, and the flange due to excessive strain loading. This effect is even more pronounced as the crack propagates further behind the fiber, resulting in an "inversion" of the signal and an increasing number of dropouts, as shown in Figure 16.

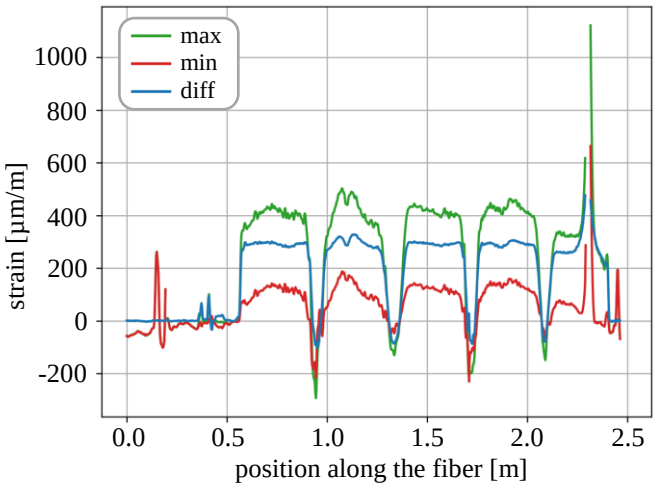

Figure 13: Subtraction of the minimum (red) and maximum (green) DFOS signal from May 9, 2023, at 10:52 to obtain the mean (blue), which was compared to the output from the numerical simulations; Q3R location.

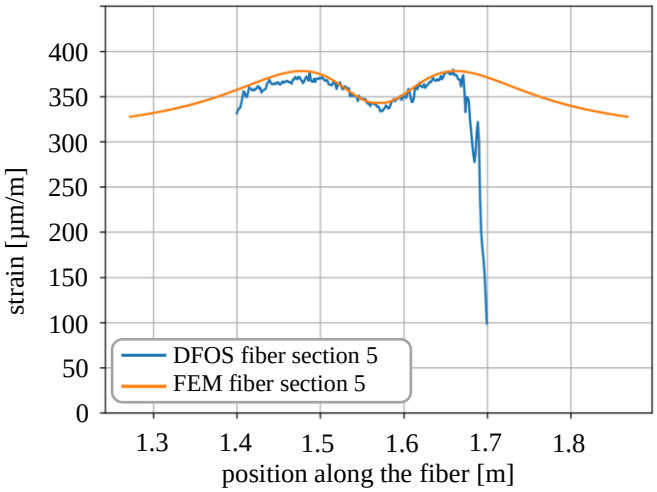

Figure 14: Comparison of the strain signal at fiber section 5 from the linear FEM simulation and the DFOS measurements taken on the sixth measurement day at the Q3R location.

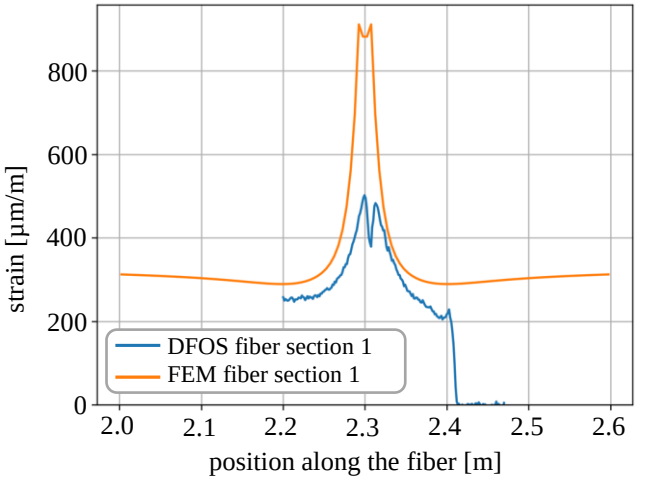

Figure 15: The crack tip near fiber section 1 causing nonlinear effect resulting in smaller strain peaks, first day of measurement at Q3R location.

DOI: 10.3217/978-3-99161-057-1-007

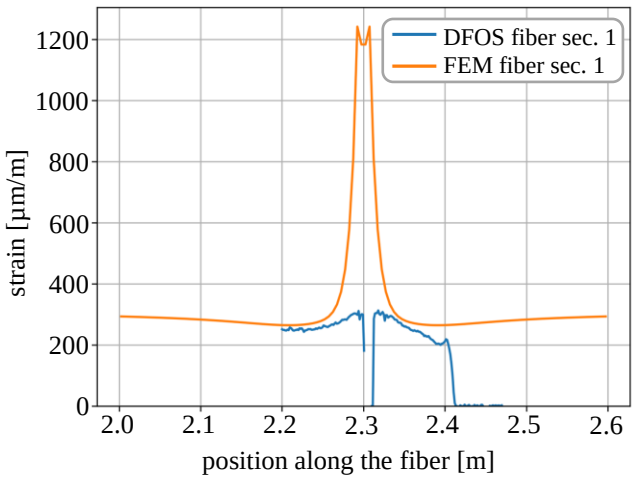

Figure 16: An "inversion" of the measured DFOS signal showing dropouts due to the wide crack opening inducing excessive strain. Third day of measurements at the Q3R location of fiber section 1.

3.4 Crack widths determined by the nonlinear model

The crack widths for the Q3L and Q3R locations were determined using the nonlinear FE hysteresis model. The following paragraphs describe the procedure at the Q3L location for fiber section 1. Here, two points in time were selected where the crack had already grown considerably, both on May 12, 2023, one at about 06:45 and one at about 10:30.

The best results were obtained in the earliest measurement because the crack widths were still not very large. The times of the maximum (load), minimum (unload) and constant load (resting state) of a cycle is considered in each loading case. At 06:41, the cyclic loading was stopped for a short time, which led to a brief complete reappearance of the DFOS strain signal. At this point, the permanent crack under constant load became very well measurable. The corresponding signal is shown in purple continuous line in Figure 17. The unloading curve (gray continuous line) is also clearly visible and shows only a few interruptions. It can be seen here that the measured values in the crack area are even slightly negative, while the areas where the load is applied remain virtually unchanged. This can be well modeled by means of the hysteresis model. It should be noted that as the crack width increases, so does the number of dropouts in the data. The loading curve (red) is only partially visible and must be reconstructed to determine the underlying area corresponding to the crack width. This is done by the accompanying FE analysis, which is shown in the Figure 17 as a dash-dotted line in the respective colors. Since the parameters of the FE model were optimized once for all processes, each recalculation only searches for the crack width that best matches the measurement data.

The crack widths, *w*, in Figure 17, indicate the crack opening at each loading phase. If *w.max* is given, it means that at an earlier point in time a larger crack caused a change in the fiber. This can be beneficial if there was no measurement at that point in time or if the signal was too disturbed to measure. In this case, the amplitudes of the crack widths are compared and validated with the results of the displacement sensors in combination with the relationship between crack length and width in Figure 11 derived from the linear 2D FEM model. They result from the differences in crack width during loading (red) and unloading (gray) and thus correspond to the change in crack width during harmonic loading. The crack width at rest (purple) should be exactly between the two values for a symmetrical load amplitude. This also makes it possible to calculate the static crack opening without harmonic excitation. The crack opening under constant load at the fiber section 1 after crack crossing is therefore 0.205 mm and the amplitude of the crack opening under cyclic loading is 0.22 mm.

The same procedure was carried out for the later measurement at 10:28, see Figure 18, whereby the crack is considerably more developed. In this case, no DFOS strain signal could be measured in the loading phase. The strain data for unloading and constant load phases was very fragmented, but could be reconstructed by numerical simulation, The resemblance to the existing data is not as good as in the previous example, which indicates that there are more extensive nonlinearities that cannot be simulated by the model that is used. Therefore, it is expected that the evaluation of the crack widths will be less accurate in this case. Despite the absence of a loading phase, the crack width could be estimated from the difference between the unloading and the constant loading phases.

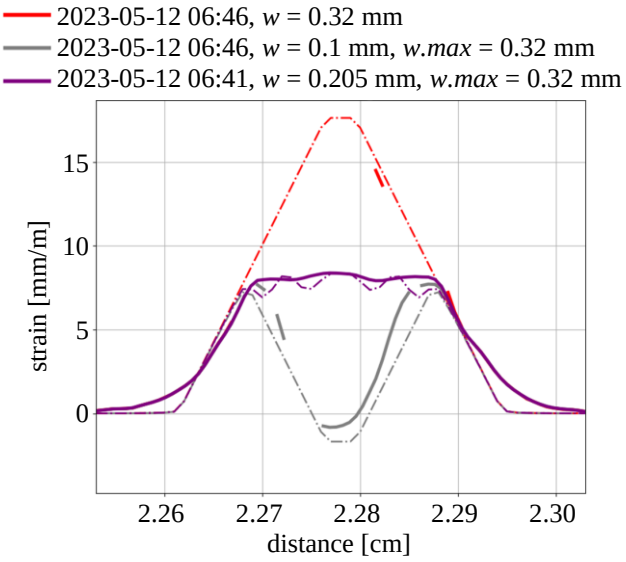

Figure 17: Matched strain signals of DFOS ("continuous lines") and the nonlinear FEM model (dash-dotted lines) for fiber section 1; measurement location Q3L; loading curves are red, unloading in gray, and constant load in purple.

4 DISCUSSION

4.1 Influence of gage pitch on dropouts

Three gage pitches (0.65 mm, 1.3 mm, and 2.6 mm) were used during the DFOS experimental campaign in order to investigate their suitability for monitoring of crack propagation under harmonic loading. Although it is recommended to use the shortest gage pitches for regions with high strain gradients [1], in this case the signal acquired with the 0.65 mm gage pitch contained the most dropouts and noise. The larger the crack opening, the more pronounced this effect was. Therefore, it was not suitable for further processing and the two longer gage pitches were preferred for evaluation as the acquired signal

DOI: 10.3217/978-3-99161-057-1-007

contained fewer dropouts, with 2.6 mm gage pitch having the fewest.

It is recognized that the situation can be remedied by using optical fibers with higher sensitivity. In [1], the authors monitored cracks in a concrete beam using four different optical fibers and gage pitch of 0.65 mm. The results emphasized the need for careful selection of optical fibers that are better suited for measuring high gradients, if case that the crack location and crack opening are to be reliably quantified.

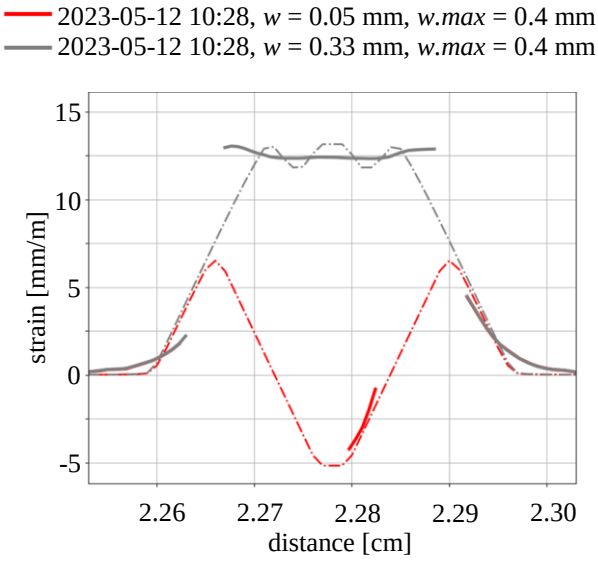

Figure 18: Matched strain signal of DFOS ("continuous lines") and the nonlinear FEM model (dash-dotted line) for fiber section 1; measurement location Q3L at 10:28; unloading curves are red, constant loading in gray.

4.2 Fiber layout – loop length and minimum fiber radius

In order to maintain the minimum fiber radius that can cause additional signal dropouts the optic fiber was laid in the following order of fiber section 1, 3, 5, 2, and 4. The lower the number, the closer the fiber section is to the flange edge and the notch. Although the length of the straight part of each fiber section was sufficient to capture the uniaxial stress state, it would be preferable to make these straight sections even longer, so the there are no sudden signal drops as it can be seen, for example, on the right hand side of the blue line in Figure 14.

4.3 Limitation of the linear FEM models

Although the handling of the 2D FEM model was significantly easier than the full-scale 3D FEM model of the main girder, significant amount of was required to correctly create the 2D FEM model. As a side effect, the contribution of the web to the stiffness of the flange in the presence of a crack was investigated. Interestingly, the web stiffening factor as a function of crack length is not monotonic. For crack lengths from 0 to 20 mm (and in the presence of the notch), the web stiffening effect slightly decreases, but from 20 mm to 150 mm, the web contributes to the overall stiffness by a factor 2.5 to 4.5, respectively.

It would be also of interest to investigate, how incorporating more construction details, e.g. constraining lateral movement of the main girder, modeling the gusset plates, or using displacement loading, would manifest itself on the web stiffening factor as well as on the overall results. However, it is anticipated that these effects are rather small and would not significantly change the results.

4.4 Validation and limitation of the nonlinear model

This study shows that the nonlinear hysteresis model is able to reproduce the measured DFOS strain signal for smaller crack widths where the interaction between the optical fiber and the flange is governed by nonlinear behavior. However, for larger crack widths, it remains subject to certain inaccuracy. The deviations increase with crack growth, indicating additional nonlinearities not represented in the model. It is therefore important to consider the expected crack widths of interest when selecting fibers. A thicker coating would smear the strain peaks around cracks over the longer part of the fiber core, resulting in lower peak values and thus preventing highly nonlinear effects from occurring.

The resulting crack widths for the two locations, the considered time instances, and the optical fibers were compiled and validated. The validation was done by comparing the crack width and crack length relationship developed from the extensometers and the linear FEM model in Figure 11 in Section 3.2. The results are summarized in Table 2 for measurement location Q3L and fiber sections 1 to 4.

For the considered time instances and the location Q3L, almost complete measured values are only available for the measurement time around 06:30. Therefore, the first validation was carried out at location Q3L for May 12, 2023, at 06:28, see third and sixth row in Table 2. The maximum deviations for this time instance are only 0.03 mm. This result is consistent with the previous findings on the accuracy of crack width measurements using DFOS in [2]. The comparison at 10:28 for the same location and measurement day shows significantly larger deviations of up to 0.09 mm.

Table 2: Comparison of the crack widths from the linear and nonlinear FEM models at Q3L location on May 12, 2023

		linear model + extensometer [mm]			
date	time (UTC)	fiber sec. 1	fiber sec. 2	fiber sec. 3	fiber sec. 4
12.05.2023	06:28	0.19	0.15	0.12	0.05
12.05.2023	10:28	0.35	0.30	0.24	0.17
		nonlinear model + DFOS [mm]			
12.05.2023	06:28	0.22	0.15	0.12	0.08
12.05.2023	10:28	0.35	0.21	0.21	0.11

4.5 Practical applicability of the crack monitoring using DFOS

The DFOS measurement technique could be implemented in real-world scenarios analogous to the current study. The fiber can be placed in different shapes around critical details of new or existing bridges if the minimum bending radius requirement is met. Since the unit cost of a basic optical fiber is relatively low, two or more parallel fibers can be used to measure a quantity to increase redundancy in case of fiber damage.

If the structure is exposed to different temperatures, temperature compensation is required. In this case, it is recommended to install a fiber for temperature measurement next to the fiber for strain measurement. The temperature sensing fiber should be able to move freely so that it is not

DOI: 10.3217/978-3-99161-057-1-007

affected by mechanical strain and can provide reliable temperature values.

One of the challenges is the risk of fiber damage during installation in the busy and harsh conditions of a construction site. To mitigate this risk, it is recommended to use a specialized company to install the fibers.

A notable practical example of the use of DFOS is on a concrete highway bridge near Aurachkirche, Austria, documented in [8]. In this pilot project, approximately 60 m of the Aurach Bridge is monitored in two 30 m long sections using 2.6 mm gage pitch. In each section, temperatures and strains were measured in the top and bottom slabs. During the observation period, several cracks were detected as a result of concrete shrinkage. The DFOS measurements also allowed to observe the crack closure due to prestressing. By integrating the area under the obtained strain signal, the crack widths were estimated, which were in line with the expectation for a prestressed concrete bridge. It was concluded that DFOS can be used to monitor important milestones in the construction process, including the development of cracks.

Another practical example is the recent installation of DFOS technology during the replacement of a railway bridge in Eschenau, Upper Austria. In this project, optical fibers will monitor temperature and strain throughout the construction process and future service life, enabling the detection of potential crack development. These examples demonstrate the growing adoption of DFOS in structural health monitoring projects and highlight the suitability of this technique for integration into routine bridge maintenance.

5 CONCLUSIONS

Based on the current study, the following conclusions are drawn: The FEM simulations fed with strain gauge and extensometer data can provide good qualitative and quantitative agreement with the measured DFOS strain signal. The simulated strain signal from the linear elastic FEM model agrees well with the measured DFOS strain signal in cases where linear elasticity governs the interaction between the optical fiber and the underlying steel flange. Once the crack is close enough to the fiber, the nonlinear effect comes into play and the nonlinear model must be used to reproduce the measured DFOS strain signal. In these cases, the nonlinear model can also be used to estimate the crack opening, see Section 2.9.

With increasing crack opening, the high strain in the optical fiber causes signal dropouts. This is usually the case when the crack has propagated well beyond the fiber.

The crack propagation can be clearly seen in the cyclic loading test using DFOS. First, the nonlinear effects come into play, which can be accompanied by some dropouts. Then, in the next phase, the peak of the measured strain signal changes to a trough so that it is "inverted" with respect to the previous state, see Figure 16.

The further away the fiber section is from the crack tip, the better the agreement between the measured and simulated strain signals was obtained. Typically, the best agreement between simulated and measured strain was observed for fiber section 5.

The DFOS have proven to be very good at determining steel strain up to crack initiation, crack detection, and crack widths up to 0.2 mm. Beyond that, the measured strain signal become more incomplete and the signal reconstruction is subject to increasing inaccuracy. This is exacerbated by dynamic excitation, which disturbs the strain signal. If large crack widths are still of interest, it is advisable to use coated fibers for such measurements, which reduces the peak strains. If the information on whether and where a crack has occurred is sufficient, simple and inexpensive commercially available fibers, such as those used in the Pinkabach Bridge tests, can provide adequate information. When more precise evaluations were required, it became apparent that the fiber had to be selected precisely according to the expected crack widths. Overall, the DFOS technique was found to be suitable for crack detection and crack propagation monitoring.

ACKNOWLEDGMENTS

The work presented here was carried out as part of the FFG COMET research project ‘Railways for Future: Resilient Digital Railway Systems to enhance performance’ (in short: Rail4Future) 882504, which was led by the Austrian Federal Railways ÖBB-Infrastruktur AG. The authors would also like to thank Alfred Lechner and Stefan Wittmann for their support with the measurements and the partners involved in the project for their excellent cooperation.

REFERENCES

[1] M. Herbers, B. Richter, und S. Marx, „Rayleigh-based crack monitoring with distributed fiber optic sensors: experimental study on the interaction of spatial resolution and sensor type“, *Journal of Civil Structural Health Monitoring*, S. 1–25, Dez. 2024, doi: 10.1007/s13349-024-00896-5.

[2] A. Vorwagner, M. Kwapisz, W. Lienhart, M. Winkler, C. Monsberger, und D. Prammer, „Verteilte Rissbreitenmessung im Betonbau mittels faseroptischer Sensorik – Neue Anwendung von verteilten faseroptischen Messsystemen“, *Beton- und Stahlbetonbau*, Bd. 116, Nr. 10, S. 727–740, 2021, doi: https://doi.org/10.1002/best.202100060.

[3] S. A. Taher *u. a.*, „Structural Health Monitoring of Fatigue Cracks for Steel Bridges with Wireless Large-Area Strain Sensors“, *Sensors*, Bd. 22, Nr. 14, Art. Nr. 14, Jan. 2022, doi: 10.3390/s22145076.

[4] W. Xu, C. Cui, C. Luo, und Q. Zhang, „Fatigue crack monitoring of steel bridge with coating sensor based on potential difference method“, *Construction and Building Materials*, Bd. 350, S. 128868, Okt. 2022, doi: 10.1016/j.conbuildmat.2022.128868.

[5] A. Mufti, D. Thomson, D. Inaudi, H. Vogel, und D. McMahon, „Crack detection of steel girders using Brillouin optical time domain analysis“, *Journal of Civil Structural Health Monitoring*, Bd. 1, Dez. 2011, doi: 10.1007/s13349-011-0006-8.

[6] K. Kishida, T. L. Aung, und R. Lin, „Monitoring a Railway Bridge with Distributed Fiber Optic Sensing Using Specially Installed Fibers“, *Sensors*, Bd. 25, Nr. 1, Art. Nr. 1, Jan. 2025, doi: 10.3390/s25010098.

[7] „Luna ODiSI 6000 Optical Distributed Sensor Interrogator“. Zugegriffen: 4. April 2025. [Online]. Verfügbar unter: https://lunainc.com/product/odisi-6000-series

[8] V. Boros, A. Vorwagner, D. Prammer, und W. Lienhart, „Application of Embedded Distributed Fiber Optic Sensors on a Highway Bridge as a Support for Bridge Inspections“, Sep. 2024.

[9] *Ansys® Mechanical APDL*, Release 17.0, Help System, Element Reference, Ansys Inc., 2015.